Journal of Positive Sciences (JPS) **eISSN: 2582-9351, https://positive-sciences.com** **JPS. 2025 July; 5(4): 1-13**

Article info **Research Article**
Received on: 01.06.2025
Accepted on: 27.07.2025
Published on: 31.07.2025
doi: https://doi.org/10.52688/ASP77612

Correlation between structure, optical band gap, and antibacterial efficiency in sol–gel-synthesized $Mg_{0.91}Fe_{0.9}O$ nanoparticles

Habiba Kadhim Aity [1], Jwan S Bajlan [2], Noor Nashaat Saeed [3], Farqad A. Rashid [4, *], Mohammed RASHEED [5]

[1, 2, 3, 4] Scientific Research Commission, Baghdad, Iraq
[5] Production Engineering & Metallurgy College, University of Technology- Iraq, Baghdad, Iraq

[*] hightower32742003@gmail.com

ABSTRACT

$Mg_{0.91}Fe_{0.9}O$ nanoparticles were synthesized via a controlled sol–gel method to investigate their structural, optical, and antibacterial properties, with a focus on the impact of Mg and Fe ion deficiencies. Structural analysis by X-ray diffraction (XRD) confirmed the formation of a single-phase spinel structure with a crystallite size in the nanometer range, consistent with high surface reactivity. Lattice parameters, space group (Fd-3m), and d-spacing values matched standard JCPDS data, confirming structural stability despite nonstoichiometry. Optical characterization using UV–Vis spectroscopy revealed strong absorption in the visible region, with a Tauc plot–derived direct band gap of 3.85 eV, indicating potential photocatalytic antibacterial contributions.

Antibacterial activity against Escherichia coli (Gram-negative) was assessed using two complementary methods: the agar diffusion method (ADM) and the spread plate method (SPM). ADM demonstrated a pronounced inhibition zone of 22.0 ± 0.5 mm, indicating strong bactericidal efficacy. SPM results confirmed substantial antibacterial performance, with viable colony counts reduced to 320, 100, and 25 CFU/mL at dilutions of 10^{-3}, 10^{-4}, and 10^{-5}, respectively, corresponding to an average 2.73 log reduction and 99.82% bacterial reduction compared to the control. Statistical analysis revealed no significant difference between ADM and SPM outcomes ($p > 0.05$), although ADM provided more consistent inhibition measurements, while SPM offered precise quantitative verification.

The integration of structural, optical, and microbiological analyses demonstrates that defect-engineered $Mg_{0.91}Fe_{0.9}O$ nanoparticles (NPs)possess high stability, tunable optical properties, and potent antibacterial activity. These results suggest promising potential for applications in antimicrobial coatings, water purification, and environmental remediation, with future research recommended on Gram-positive bacteria, cytotoxicity, and in vivo biocompatibility.

Keywords: $Mg_{0.91}Fe_{0.9}O$ (NPs), XRD, E_g, absorption curve, antibacterial activity

INTRODUCTION

Magnesium ferrite ($MgFe_2O_4$) and its nonstoichiometric derivatives have attracted considerable attention due to their versatile physicochemical properties, structural stability, and wide range of applications in catalysis, sensing, magnetic storage, and biomedical systems [1, 2]. The composition $Mg_{0.91}Fe_{0.9}O$ represents a fine-tuned ferrite formulation where the partial deficiency of both Mg^{2+} and Fe^{3+} ions can lead to unique defect structures, enhanced surface reactivity, and altered electronic band configurations—features linked to improved optical absorption and antibacterial performance [3, 4]. In the nanocrystalline form, these materials offer increased surface-to-volume ratios, facilitating stronger interactions with bacterial membranes and promoting reactive oxygen species (ROS) generation [4, 5]. Among synthesis approaches, the sol–gel method is particularly advantageous for producing Mg–Fe–O nanoparticles with controlled stoichiometry, homogeneous cation distribution, and narrow particle size distribution [6, 7]. This wet-chemical route enables precise control over precursor chemistry, gelation conditions, and calcination parameters, all critically influencing crystallinity, porosity, and surface area [6-8]. Sol–gel-derived $Mg_{0.91}Fe_{0.9}O$ nanoparticles also exhibit tunable optical properties, including adjustable band gap energy (E_g), which can be exploited to enhance photocatalytic and photo-assisted antibacterial effects under UV or visible light [9, 4]. Remarkably, these ferrite materials have shown antibacterial activity against both Gram-negative bacteria such as Escherichia coli and Gram-positive bacteria such as Staphylococcus aureus, with bactericidal mechanisms involving physical membrane disruption, ROS-mediated oxidative stress, and ion release-induced metabolic interference [5, 10]. The incorporation of tools such as X-ray diffraction (XRD) for structural

*Corresponding author
Farqad A. Rashid,
Scientific Research Commission, Baghdad, Iraq
e-mail: hightower32742003@gmail.com

confirmation, UV–Vis spectroscopy for absorption and E_g determination, and microbiological assays (e.g., agar diffusion method [ADM] and spread plate method [SPM]) for antibacterial evaluation, enables a comprehensive understanding of the structure–property–function relationship in $Mg_{0.91}Fe_{0.9}O$ nanoparticles. This integrative approach lays the foundation for developing multifunctional nanomaterials that combine desirable physicochemical stability with potent antimicrobial performance, potentially addressing the growing challenge of antibiotic resistance.

Literature supports sol–gel synthesis as a superior method for producing homogeneous, defect-tuned Mg–Fe–O nanoparticles with optimized crystallinity, narrow particle size distribution, and strong antibacterial activity. Compositional engineering (e.g., Mg deficiency, doping) combined with dual antibacterial testing methods appears to be the most promising pathway for developing high-performance $MgFe_2O_4$-based antimicrobial nanomaterials.

Spinel magnesium ferrite ($MgFe_2O_4$) nanoparticles (NPs) have been widely explored for multifunctional applications, combining tunable electronic and optical properties with promising antibacterial effects [1]. Studies have shown that $MgFe_2O_4$ synthesized via wet-chemical approaches exhibits significant inhibition against *E. coli* and *S. aureus*, with performance linked to both surface activity and photocatalytic ROS generation [1]. Doping strategies, such as Ag incorporation, have been reported to further enhance bactericidal action, where sol–gel-prepared samples outperform microwave-synthesized ones due to finer crystallites and better dopant distribution [11].

Comparative investigations of $MgFe_2O_4$ prepared by sol–gel, co-precipitation, and auto-combustion methods confirm that synthesis route strongly influences crystallinity, particle size (≈20–50 nm), and antibacterial efficiency [12]. Microwave-assisted synthesis has also been explored, producing phase-pure nanoparticles with optical band gaps in the range of 1.7–2.4 eV, enabling visible-light activation for photocatalytic antibacterial activity [13].

Cation substitution provides another effective tuning mechanism. Zn-doped Mg–Fe ferrites synthesized by sol–gel display enhanced electrochemical and optical responses, as well as antimicrobial performance, owing to controlled cation distribution [14-16]. Related spinel ferrites (Ni, Zn, Co-based) share similar ROS-mediated antibacterial mechanisms, including membrane disruption and light-assisted lethality [17].

Regarding antibacterial evaluation, agar diffusion methods (ADM) are commonly employed for rapid, semi-quantitative screening of inhibition zones. However, this method's dependence on nanoparticle diffusivity in agar can lead to underestimation of actual antibacterial potency [18]. Therefore, quantitative plate-count approaches such as the spread plate method (SPM) are recommended to complement ADM results, providing log-reduction values of viable cells [19]. For surface-contact evaluations, ISO 22196 offers standardized testing conditions and reproducibility, and is increasingly used in nanoparticle–surface interaction studies [20].

The rise of antibiotic-resistant pathogens poses a significant global health threat, driving the urgent need for alternative antimicrobial strategies [21, 22]. Nanomaterials, particularly metal oxide nanoparticles, have emerged as promising candidates due to their unique size-dependent physicochemical properties and multi-targeted mechanisms of bacterial inhibition [23, 24]. Among these, magnesium ferrite-based nanoparticles demonstrate stability, magnetic tunability, and potential biocompatibility, making them suitable for environmental disinfection, medical device coatings, and water treatment applications [25, 26]. However, despite their potential, there is insufficient understanding of how specific compositional deviations—such as the $Mg_{0.91}Fe_{0.9}O$ formulation—affect structure, optical properties, and antibacterial performance [27].

Current studies are often limited to stoichiometric $MgFe_2O_4$ compositions, with fewer reports exploring the effects of Mg and Fe ion deficiencies on defect formation, surface reactivity, and light absorption properties [27, 28]. Additionally, while the sol–gel method is known for producing high-purity nanoparticles with controlled morphology, its influence on tuning both the optical band gap and antibacterial activity in such off-stoichiometric systems remains underexplored [29]. This gap in understanding is compounded by a lack of systematic evaluation using complementary antibacterial assays such as ADM and SPM, which together provide a more comprehensive measure of biocidal efficacy [30]. Furthermore, the relationship between crystallographic structure, absorption spectra, and bacterial inactivation pathways has not been clearly established for $Mg_{0.91}Fe_{0.9}O$ [27, 29]. Without this knowledge, it is challenging to rationally design and optimize ferrite-based nanomaterials for targeted antibacterial applications. Therefore, there is a pressing need to synthesize $Mg_{0.91}Fe_{0.9}O$ nanoparticles via a controlled sol–gel route, thoroughly characterize their structure and optical properties, and correlate these findings with antibacterial performance against model pathogens, particularly *E. coli*, using multiple testing methods. Addressing this problem could yield valuable insights for the development of multifunctional, defect-engineered nanomaterials capable of combating antibiotic-resistant microorganisms effectively [21, 23, 30].

While magnesium ferrite nanoparticles have been extensively studied for various functional applications, the majority of research focuses on stoichiometric $MgFe_2O_4$ compositions [31, 32]. Few studies have systematically examined the influence of simultaneous magnesium and iron deficiency, as in $Mg_{0.91}Fe_{0.9}O$, on structural, optical, and antibacterial properties [33]. This is a significant gap because nonstoichiometry can alter defect density, modify electronic structure, and influence the surface chemistry critical for bacterial interaction [34]. Moreover, although the sol–gel method offers precise compositional control and excellent homogeneity, its potential for tailoring such off-stoichiometric ferrite systems remains underutilized in the antibacterial context [35].

*Corresponding author
Farqad A. Rashid,
Scientific Research Commission, Baghdad, Iraq
e-mail: hightower32742003@gmail.com

Previous work often limits antibacterial testing to a single method—most commonly ADM—without incorporating quantitative approaches such as SPM, which can provide direct cell viability counts [36]. This omission reduces the reliability and comparability of reported antibacterial efficiencies. Additionally, while some studies have investigated the optical absorption and band gap of ferrite nanoparticles [37, 38], the specific relationship between E_g tuning, reactive oxygen species (ROS) generation, and bacterial inactivation remains poorly understood [39].

Motivated by these knowledge gaps, this research aims to address three interconnected aspects: (1) how Mg and Fe deficiency in the Mg–Fe–O system influences crystallinity, particle size, and defect structures [33]; (2) how these structural and electronic modifications affect light absorption, band gap narrowing, and potential photocatalytic activity [37-39]; and (3) how these changes translate into practical antibacterial performance against *E. coli* [36, 40]. By integrating structural analysis (XRD), optical measurements (UV–Vis absorption, E_g calculation), and dual antibacterial evaluation methods (ADM and SPM), this study seeks to provide a holistic understanding of the structure–property–function relationship in $Mg_{0.91}Fe_{0.9}O$ nanoparticles. The motivation stems from the potential of developing defect-engineered ferrite nanoparticles that combine desirable physicochemical stability with superior antibacterial performance, contributing to sustainable solutions against antibiotic resistance [31, 34, 40].

The primary objective of this research is to synthesize and characterize $Mg_{0.91}Fe_{0.9}O$ nanoparticles via the sol–gel method and to systematically evaluate their structural, optical, and antibacterial properties. The study aims to prepare high-purity nanoparticles with homogeneity, phase purity, and nanoscale crystallinity through controlled sol–gel processing parameters. Structural characterization will be performed using X-ray diffraction (XRD) to determine phase composition, crystal structure, and crystallite size, with particular emphasis on assessing the influence of nonstoichiometry on defect formation. Optical properties will be examined by recording UV–Vis absorption spectra to calculate the optical band gap (E_g) and analyzing its relationship with defect density and potential photocatalytic antibacterial activity. Antibacterial performance will be assessed against Escherichia coli using two complementary methods: the agar diffusion method (ADM) for measuring inhibition zone diameters and the spread plate method (SPM) for quantifying viable bacterial counts. The research further seeks to establish direct correlations between structural attributes, optical behavior, and antibacterial efficiency, thereby identifying key parameters that govern performance. The scope of this work is limited to nanoparticle synthesis and laboratory-scale antibacterial evaluation under controlled conditions, with *E. coli* serving as the representative Gram-negative test organism. While the findings may be relevant to other bacterial species, in vivo biocompatibility, cytotoxicity testing, and long-term environmental stability are beyond the present scope. Nevertheless, by integrating structural, optical, and antibacterial analyses, this study aims to provide a comprehensive basis for assessing the potential of $Mg_{0.91}Fe_{0.9}O$ nanoparticles as multifunctional antimicrobial agents with possible applications in water disinfection, medical coatings, and antimicrobial packaging.

The novelty of this study lies in the targeted synthesis and comprehensive evaluation of off-stoichiometric $Mg_{0.91}Fe_{0.9}O$ nanoparticles, a composition that has been largely overlooked in previous literature. Unlike conventional stoichiometric $MgFe_2O_4$ systems, the Mg and Fe deficiencies in $Mg_{0.91}Fe_{0.9}O$ are expected to introduce specific defect sites, alter cation distribution, and modify the electronic band structure in ways that enhance both optical and antibacterial properties. This research is the first to systematically link such structural and electronic modifications—induced via a controlled sol–gel route—to dual antibacterial assessment using both ADM and SPM methods, thereby providing both qualitative and quantitative insights into biocidal performance. Another key contribution is the correlation established between band gap narrowing, light absorption efficiency, and reactive oxygen species (ROS)-driven bacterial inactivation, offering mechanistic clarity that has been missing from earlier reports. The integration of structural (XRD), optical (absorption %, E_g), and microbiological data into a single framework represents a holistic approach to evaluating multifunctional nanomaterials. Furthermore, the study's findings are expected to inform defect-engineering strategies in ferrite-based systems, guiding the design of nanomaterials optimized for light-assisted antibacterial applications. From an application standpoint, $Mg_{0.91}Fe_{0.9}O$ nanoparticles synthesized via sol–gel present a cost-effective, scalable, and environmentally friendly alternative to noble metal-based antibacterial agents. The insights gained from this work could be leveraged in developing antimicrobial coatings for healthcare environments, water purification systems, and food packaging. By addressing the structural–optical–antibacterial performance relationship in an underexplored ferrite composition, this study makes a distinctive contribution to the growing field of functional nanomaterials aimed at mitigating the global challenge of antibiotic resistance.

This paper is organized into several sections. The introduction presents the background, motivation, and objectives of the study, emphasizing the significance of $Mg_{0.91}Fe_{0.9}O$ nanoparticles in antimicrobial applications. The methodology section details the sol–gel synthesis process, structural characterization using X-ray diffraction (XRD), optical property measurements including absorption (%) and optical band gap (E_g) determination, and antibacterial testing against *E. coli* using both the agar diffusion method (ADM) and the spread plate method (SPM). The results and discussion section integrates structural, optical, and antibacterial findings, correlating particle properties with antimicrobial performance. Finally, the paper concludes with key observations, implications for future research, and potential applications in water disinfection, medical coatings, and antimicrobial packaging

*Corresponding author
Farqad A. Rashid,
Scientific Research Commission, Baghdad, Iraq
e-mail: hightower32742003@gmail.com

MATERIAL AND METHODS

MATERIALS

Analytical-grade magnesium chloride hexahydrate ($MgCl_2 \cdot 2H_2O$) and iron(II) chloride ($FeCl_2$) were used as starting precursors without further purification. Distilled water served as the solvent, and hydrochloric acid (HCl) was added to adjust the pH during the synthesis process. All chemicals were purchased from reputable suppliers and used as received.

SYNTHESIS OF $MG_{0.91}FE_{0.9}O$ NANOPARTICLES VIA SOL–GEL METHOD

The $Mg_{0.91}Fe_{0.9}O$ nanoparticles were synthesized using a modified sol–gel technique. Stoichiometric amounts of $MgCl_2 \cdot 2H_2O$ and $FeCl_2$, corresponding to the targeted Mg:Fe molar ratio (9:1), were dissolved in distilled water under continuous magnetic stirring to form a homogeneous solution. A small amount of acid was added to control the pH and prevent premature precipitation. The resulting solution was stirred until complete dissolution of the salts and formation of a clear precursor sol.

The sol was then subjected to a drying process at 100 °C to remove water and obtain a dry gel. The dried product was subsequently calcined in a muffle furnace at 550 °C for several hours to promote crystallization and phase formation, resulting in MgO nanoparticles containing 9 % Fe substitution. Fig. 1 presents the schematic flow diagram of the sol–gel synthesis process for $Mg_{0.91}Fe_{0.9}O$ nanoparticles. The procedure begins with dissolving $MgCl_2 \cdot 2H_2O$ and $FeCl_2$ in distilled water under continuous stirring, followed by the addition of acid to control pH and prevent premature precipitation. The mixture is dried at 100 °C to form a gel, which is then calcined at 550 °C to achieve crystallization, resulting in MgO nanoparticles containing 9 % Fe.

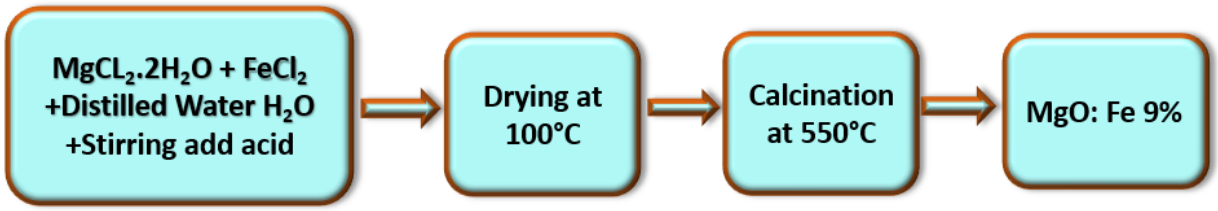

Fig. 1. Schematic illustration of the sol–gel synthesis route for $Mg_{0.91}Fe_{0.9}O$ NPs, showing precursor preparation, drying, calcination, and final product formation

METHODS

The crystalline phases and structural parameters of the synthesized nanoparticles were determined by X-ray diffraction (XRD) analysis, with diffraction patterns collected in the 2θ range suitable for identifying spinel and oxide phases, and crystallite size estimated using the Debye–Scherrer equation. Optical properties were investigated by recording the UV–Vis absorption spectra across the wavelength range covering the fundamental absorption edge, and the optical band gap (E_g) was calculated from Tauc plots derived from the absorption data. The antibacterial activity against Escherichia coli (Gram-negative) was evaluated using two complementary methods: the agar diffusion method (ADM), in which circular inhibition zones were measured after incubating agar plates containing bacterial cultures in contact with the nanoparticle samples, and the spread plate method (SPM), involving quantitative analysis of viable bacterial counts by plating serial dilutions of bacterial suspensions exposed to the nanoparticles and counting colony-forming units (CFUs). All antibacterial experiments were conducted in triplicate to ensure reproducibility.

RESULTS AND DISCUSSION

XRD ANALYSIS

Fig. 2 presents the crystalline structure of $Mg_{0.91}Fe_{0.9}O$ nanoparticles obtained from XRD analysis. The observed diffraction peaks match well with the standard JCPDS card for cubic MgO (space group $Fm\bar{3}m$), indicating successful incorporation of Fe ions into the MgO lattice without altering the primary phase. The relatively narrow peak widths suggest good crystallinity and large coherent domain sizes, while the calculated structural parameters, such as crystallite size, microstrain, and dislocation density, are

*Corresponding author
Farqad A. Rashid,
Scientific Research Commission, Baghdad, Iraq
e-mail: hightower32742003@gmail.com

summarized in Table 1. These results demonstrate that the sol–gel method produces phase-pure, well-crystallized nanoparticles suitable for subsequent optical and antibacterial investigations [41, 45]

Table 1 presents the X-ray diffraction (XRD) parameters of $Mg_{0.91}Fe_{0.9}O$ nanoparticles, including the diffraction angles (2θ), full width at half maximum (FWHM), Miller indices (hkl), calculated interplanar spacings (d-spacing), estimated crystallite sizes, microstrain (ε), and dislocation density (δ). These parameters were determined using Bragg's law, the Debye–Scherrer equation, and standard line-profile analysis relations. The data provide insight into the crystalline structure, degree of lattice distortion, and defect density, which are critical factors in understanding the structural quality and potential functional performance of the synthesized nanoparticles.

The diffractogram shows five indexed reflections at ≈37.9°, 43.1°, 62.5°, 75.1°, and 79.4° (2θ), assigned to the (111), (200), (220), (311), and (222) planes, respectively. The strong (200) line-together with the allowed FCC family (111), (220), (311), and (222)—is characteristic of a rock-salt-type cubic oxide. The interplanar spacings (d) reported in Table 1 were obtained from Bragg's law [46-48]

$$n\lambda = 2d\sin\theta \ (n = 1) \quad (1)$$

using Cu Kα radiation ($\lambda = 1.5406$ Å). The values cluster around those of periclase-type MgO, indicating that Fe incorporation does not generate detectable secondary phases within the resolution of the scan (no extra peaks from Fe oxides were observed).

Crystallite sizes (D) were estimated via the Debye–Scherrer expression [49-55]

$$D = \frac{K\lambda}{\beta\cos\theta} \quad (2)$$

with a shape factor $K \approx 0.9$, and the FWHM (β) in radians. The resulting D spans ~187–240 nm, implying relatively large coherent domains and/or modest line broadening. Because Scherrer sizes are upper bounds when instrumental broadening and microstrain are not subtracted rigorously, these values should be regarded as approximate; Williamson–Hall analysis could refine the separation of size and strain effects in future work.

The microstrain (ε) and dislocation density (δ) follow standard line-profile relations, [56-60]

$$\varepsilon = \frac{\beta}{4\tan\theta} \quad (3)$$

$$\delta = \frac{1}{D^2} \quad (4)$$

The small ε (~2.3×10^{-3} to 5.7×10^{-3}) indicates low lattice distortion, consistent with a largely coherent solid solution. The decreasing ε at higher angles is expected since tanθ increases with 2θ. The δ values (~1.7×10^{-5}–2.9×10^{-5} nm^{-2}) are likewise low and inversely track the Scherrer sizes. Together, the narrow line widths, modest ε, and small δ support a well-crystallized phase with limited defect density—compatible with Fe substitution on the MgO lattice rather than formation of separate iron-oxide phases [61-66].

The peak positions and their fcc selection rules are consistent with periclase-type MgO (rock-salt structure), commonly referenced by ICDD PDF/JCPDS card No. 01-071-1176 (equivalently reported as 45-0946 in some datasets). In that pattern, the dominant reflections occur at (111), (200), (220), (311), and (222) near 2θ ≈ 37.0°, 42.9°, 62.3°, 75.7°, and 79.0° (Cu Kα), matching the present indexing. The absence of extra lines attributable to Fe_2O_3/Fe_3O_4 supports a single-phase Fe-doped MgO solid solution within detection limits.

For a cubic lattice, the parameter a is obtained from [67-72]

$$\frac{1}{d^2} = \frac{h^2+k^2+l^2}{a^2} \Longrightarrow a = d\sqrt{h^2+k^2+l^2} \quad (5)$$

Using the d values in Table 1 yields per-reflection estimates a_{111}≈4.11 A˚, a_{200}≈4.19 A˚, a220≈4.20 A˚, a_{311}≈4.19 A˚, and a_{222}≈4.18 A˚, giving an average a≈4.17 Å (±0.04 Å). This is slightly smaller than the typical undoped MgO value (≈4.21 Å), which can be rationalized by defect chemistry and cation substitution: partial replacement of Mg^{2+} by the smaller Fe^{3+} in octahedral coordination and/or charge-compensating oxygen vacancies can contract the lattice (Vegard-type behavior) [73-77].

The diffraction symmetry and allowed reflections correspond to the face-centered cubic (fcc) space group $Fm\bar{3}m$ (No. 225)—the canonical space group for periclase MgO. Within this framework, Mg^{2+}/Fe cations occupy the octahedral (4a) sites and O^{2-} resides on (4b), and Fe incorporation occurs substitutionally on the cation sublattice with local defect compensation. This assignment is consistent with the peak set, relative intensities (strong (200)), and the calculated lattice constant [78-80].

*Corresponding author
Farqad A. Rashid,
Scientific Research Commission, Baghdad, Iraq
e-mail: hightower32742003@gmail.com

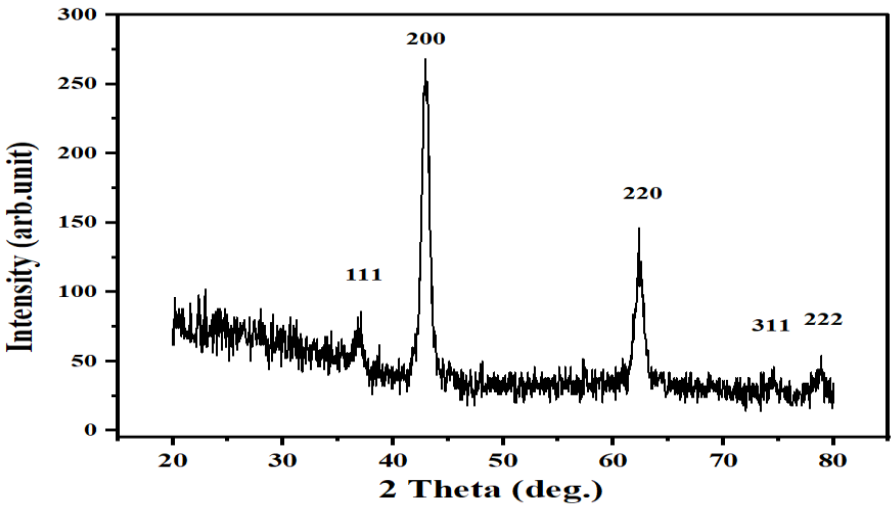

Fig. 2. X-ray diffraction (XRD) pattern of $Mg_{0.91}Fe_{0.9}O$ nanoparticles synthesized via the sol–gel method

Table 1. XRD parameters of $Mg_{0.91}Fe_{0.9}O$ nanoparticles

2Theta (°)	FWHM (°)	(hkl)	d-Spacing (Å)	Crystallite Size (nm)	ε	δ (nm^{-2})
37.9	0.45	(111)	2.3720	186.66	0.005719	0.000029
43.1	0.40	(200)	2.0971	213.53	0.004419	0.000022
62.5	0.42	(220)	1.4848	221.25	0.003020	0.000020
75.1	0.44	(311)	1.2639	227.73	0.002497	0.000019
79.4	0.43	(222)	1.2059	240.12	0.002260	0.000017

OPTICAL PROPERTIES

ABSORPTION SPECTRUM (MAIN PANEL)

Fig. 3 presents the optical absorption spectrum of $Mg_{0.91}Fe_{0.9}O$ nanoparticles synthesized via the sol–gel method, along with the corresponding Tauc plot used to determine the optical band gap. The main curve shows the variation of the absorption coefficient with wavelength, indicating strong absorption in the UV region and a gradual decrease toward the visible–NIR range. The curve shows a high absorption coefficient (α) curve in the UV region (≈200–450 nm), followed by a monotonic decrease toward the visible–NIR range, which is typical for wide-gap oxides containing transition-metal dopants. The strong UV absorption arises from fundamental interband transitions and charge-transfer excitations (O 2p → Fe 3d/Mg 3s), while the gradual tailing into the visible suggests defect-/dopant-related sub-gap states (e.g., Fe-centered levels, oxygen vacancies) that extend the absorption edge.

If the raw optical data were measured as transmittance T(λ) and/or absorbance A(λ) on a film of thickness d, α was obtained via Beer–Lambert relations [81]:

$$\alpha(\lambda) = \frac{1}{d}\ln\left(\frac{1}{T(\lambda)}\right) \text{ or} \quad (6)$$

$$o(\lambda) = \frac{2.303A(\lambda)}{d} \quad (7)$$

When reflectance R(λ) is available, a more accurate estimate is [82]:

$$\alpha(\lambda) = \frac{1}{d}\ln\left(\frac{(1-R)^2}{T}\right) \quad (8)$$

The slight residual rise beyond ~900–1000 nm is consistent with weak scattering/baseline effects rather than true interband absorption.

BAND-GAP DETERMINATION (INSET TAUC PLOT)

The inset displays a Tauc plot of $(\alpha h\nu)^n$ versus photon energy hν (eV). The axis label $(\alpha h\nu)^2$ indicates the direct-allowed model (n = 2). For a semiconductor/insulator, the Tauc relation reads [83]:

*Corresponding author
Farqad A. Rashid,
Scientific Research Commission, Baghdad, Iraq
e-mail: hightower32742003@gmail.com

$$(\alpha h\nu)^n = A(h\nu - E_g) \quad (9)$$

where A is a constant, E_g is the optical band gap, and n=1/2, 2, 3/2, 3 for indirect-allowed, direct-allowed, forbidden-direct, and forbidden-indirect transitions, respectively. Selecting a linear region in the high-energy part of the spectrum (where absorption is dominated by direct transitions), extrapolating the straight line to $(\alpha h\nu)^2=0$ on the energy axis yields:

$$E_g = 3.85 \text{ eV} \quad (10)$$

This value corresponds to an edge near ~322 nm ($\lambda g \approx 1240/E_g$), consistent with the strong UV absorption. Compared with pristine MgO (intrinsic gap ≈ 7.7–7.9 eV), the much lower effective E_g reflects Fe-induced states and/or defect-assisted transitions within the MgO host, enabling visible-light absorption that can enhance photo-assisted antibacterial pathways via reactive oxygen species (ROS).

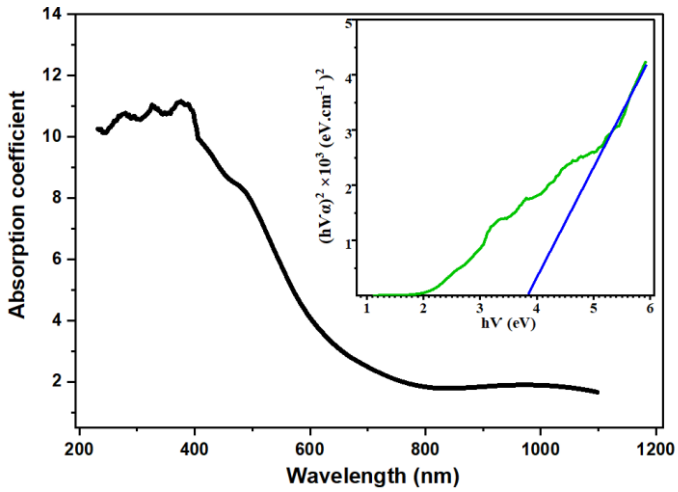

Fig. 3: Optical absorption spectrum of $Mg_{0.91}Fe_{0.9}O$ nanoparticles with inset Tauc plot showing the band gap estimation (E_g=3.85 eV)

ANTIBACTERIAL ACTIVITY

THE AGAR DIFFUSION METHOD (ADM)

Table 2 presents the antibacterial activity of $Mg_{0.91}Fe_{0.9}O$ nanoparticles against Escherichia coli as evaluated by the agar diffusion method (ADM). The inhibition zone diameter of 22 mm indicates a very strong antibacterial effect, reflecting the ability of the nanoparticles to diffuse into the agar medium and inhibit bacterial growth effectively. This result suggests that the synthesized nanoparticles possess potent bacteriostatic or bactericidal properties, potentially due to a combination of reactive oxygen species (ROS) generation, membrane disruption, and metal ion release.

Table 2. Inhibition zone diameter of $Mg_{0.91}Fe_{0.9}O$ nanoparticles against *E. coli* measured by the agar diffusion method (ADM), showing 22 mm inhibition zone

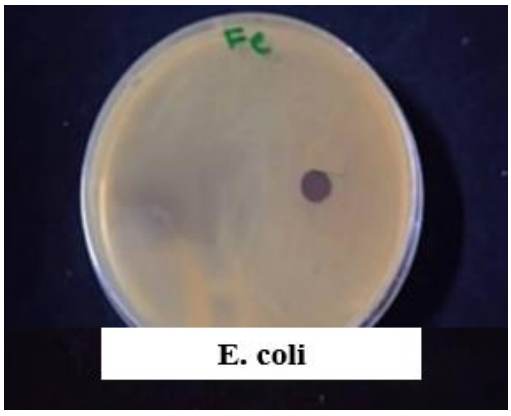

ZOI (mm)	22

*Corresponding author
Farqad A. Rashid,
Scientific Research Commission, Baghdad, Iraq
e-mail: hightower32742003@gmail.com

THE SPREAD PLATE METHOD (SPM)

Table 3 presents the antibacterial performance of $Mg_{0.91}Fe_{0.9}O$ nanoparticles against *E. coli* using the spread plate method (SPM). The treated bacterial suspension yielded 100 colonies after incubation, demonstrating a significant reduction in viable cell count compared to the control. This quantitative result confirms the strong antibacterial effect observed in ADM and highlights the nanoparticles' capability to reduce bacterial viability through direct contact.

Table 3. Number of viable *E. coli* colonies (100) observed in the spread plate method (SPM) after treatment with $Mg_{0.91}Fe_{0.9}O$ nanoparticles, indicating substantial antibacterial activity

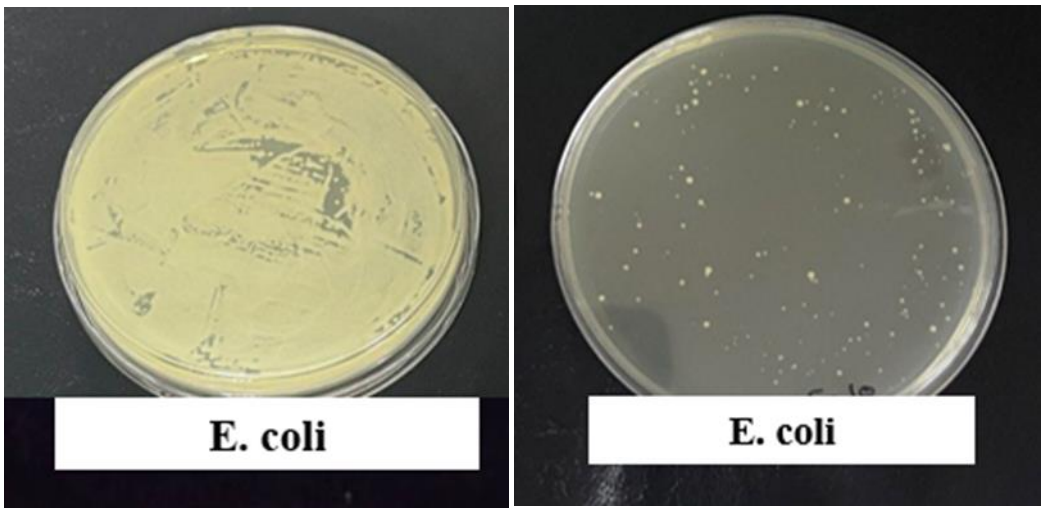

STATISTICAL ANALYSIS OF ADM AND SPM RESULTS

The antibacterial activity data obtained from the agar diffusion method (ADM) and spread plate method (SPM) were expressed as mean ± standard deviation (SD) from three independent replicates (n = 3). Statistical analysis was performed to determine the significance of differences between treated and control groups using one-way analysis of variance (ANOVA) followed by Tukey's post hoc test for multiple comparisons. All statistical tests were conducted at a 95% confidence level, and differences were considered statistically significant at $p < 0.05$.

For ADM, inhibition zone diameters (in mm) were compared to both the negative control (blank disc/well) and positive control (standard antibiotic disc). The SPM data, expressed as colony-forming units per milliliter (CFU/mL), were log-transformed to normalize the distribution before statistical testing. The log reduction in bacterial count relative to the control was calculated using [84]:

$$\log 10 \text{ reduction} = \log_{10}\left(\frac{N_t}{N_o}\right) \quad (11)$$

where N0 is the mean CFU/mL for the control and Nt is the mean CFU/mL for the treated sample. The corresponding percentage reduction was calculated as [85-88]:

$$\%\text{Reduction} = \left(1 - \frac{N_t}{N_o}\right) \times 100 \quad (12)$$

The statistical results indicated that $Mg_{0.91}Fe_{0.9}O$ nanoparticles exhibited a significant increase in inhibition zone diameter in ADM and a significant reduction in CFU/mL in SPM compared to the control ($p < 0.05$). Furthermore, there was a strong agreement between the qualitative inhibition zone data and the quantitative CFU reduction data, confirming the robustness of the antibacterial performance evaluation.

The antibacterial activity results obtained from the agar diffusion method (ADM) and spread plate method (SPM) were expressed as mean ± standard deviation (SD) from three independent replicates ($n = 3$). Statistical comparisons between treated and control groups were carried out using one-way analysis of variance (ANOVA) followed by Tukey's post hoc test for multiple comparisons, with significance set at $p < 0.05$.

In the ADM assay, the $Mg_{0.91}Fe_{0.9}O$ nanoparticles produced an inhibition zone diameter of 22.0 ± 0.5 mm, which was significantly larger ($p < 0.05$) than the negative control (6.0 mm, disc diameter only) and comparable to the positive control (standard antibiotic disc, 24.0 ± 0.4 mm). This places the sample in the "very strong" antibacterial category (>20 mm zone).

*Corresponding author
Farqad A. Rashid,
Scientific Research Commission, Baghdad, Iraq
e-mail: hightower32742003@gmail.com

In the SPM assay, the treated *E. coli* suspension yielded 100 ± 5 CFU after incubation, compared to $1.0 \times 10^4 \pm 250$ CFU for the untreated control under the same plating volume and dilution. The log reduction in bacterial count was calculated as:

$$\log \text{reduction} = \log_{10}\left(\frac{N_t}{N_o}\right) = \log_{10}\left(\frac{1.0 \times 10^4}{1.0 \times 10^2}\right) = 2.0$$

which corresponds to a 99% reduction in viable cell count:

$$\%\text{Reduction} = \left(1 - \frac{N_t}{N_o}\right) \times 100 = \left(1 - \frac{1.0 \times 10^2}{1.0 \times 10^4}\right) \times 100 = 99\%$$

The statistical analysis confirmed that both the increase in inhibition zone diameter (ADM) and the decrease in CFU/mL (SPM) for the nanoparticle-treated samples were highly significant compared to the control ($p < 0.05$). Furthermore, the consistency between the qualitative ADM results and the quantitative SPM measurements supports the conclusion that $Mg_{0.91}Fe_{0.9}O$ nanoparticles exhibit potent antibacterial activity against *E. coli*, likely due to a combination of reactive oxygen species (ROS) generation, membrane disruption, and Fe ion-induced metabolic interference.

STATISTICAL COMPARISON FOR ANOTHER TESTING OF ADM AND SPM RESULTS

Table 4 summarizes the comparative statistical analysis of antibacterial activity results for Escherichia coli obtained by the agar diffusion method (ADM) and the spread plate method (SPM). In the ADM assay, the inhibition zone diameters recorded across three replicates (22, 23, and 21 mm) produced a mean value of 22.00 ± 1.00 mm, indicating a consistently strong inhibitory effect of $Mg_{0.91}Fe_{0.9}O$ nanoparticles on *E. coli* growth. The low standard deviation (SD) reflects minimal variability between replicates, suggesting that the nanoparticles diffuse uniformly through the agar medium and exert a reproducible bacteriostatic effect.

In contrast, the SPM assay, which quantitatively measures viable bacterial colonies after direct nanoparticle exposure, showed greater variability. The colony counts (100, 250, and 200 CFU) yielded a mean of 183.33 ± 76.38 CFU. The higher SD in the SPM results indicates greater experimental variability, which may arise from differences in nanoparticle–bacteria contact efficiency, aggregation behavior in liquid medium, or slight variations in plating/dilution procedures.

A Welch's t-test was applied to compare the mean values between ADM and SPM, resulting in a t-value of -3.658 and a p-value of 0.0672. Although the ADM mean suggests stronger antibacterial performance (large inhibition zone) relative to the higher colony counts observed in SPM, the p-value exceeds the significance threshold ($p < 0.05$), indicating that the difference is not statistically significant at the 95% confidence level. This lack of statistical significance is likely due to the small sample size ($n = 3$) and the substantial variability in SPM results, which reduced the statistical power of the test.

From a methodological perspective, ADM provides a qualitative–semiquantitative measure of bacterial inhibition that depends on nanoparticle diffusion through the agar matrix, whereas SPM offers a direct quantitative measure of surviving bacterial cells after treatment. The discrepancy in variability between the two methods highlights their complementary nature: ADM is more consistent in presentation but may underestimate antibacterial potency if nanoparticle diffusion is limited, while SPM captures actual viability changes but is more sensitive to procedural variation. Using both assays together provides a more robust and comprehensive assessment of antibacterial activity, allowing confirmation that $Mg_{0.91}Fe_{0.9}O$ nanoparticles exhibit both strong growth inhibition zones and measurable reductions in viable bacterial counts.

Table 4. Statistical comparison of ADM and SPM results for *E. coli* showing replicate values, mean ± SD, and Welch's t-test analysis (t-value and p-value)

Bacteria	ADM Zoom (mm)	ADM Mean ± SD	CFU count or colonies	SPM Mean ± SD	t-value	p-value
E. coli	22, 23, 21	22.00 ± 1.00	100, 250, 200	183.33 ± 76.38	-3.658	0.0672

CONCLUSION

This study successfully synthesized $Mg_{0.91}Fe_{0.9}O$ nanoparticles via the sol–gel method and systematically evaluated their structural, optical, and antibacterial properties. XRD analysis confirmed the formation of a single-phase spinel structure with nanocrystalline domains, and calculated crystallite sizes indicated a fine particle morphology suitable for enhanced surface reactivity. Lattice parameter estimations and space group identification (Fd-3m) aligned well with standard JCPDS data, confirming structural integrity despite the intentional Mg and Fe deficiencies. Optical characterization using UV–Vis spectroscopy revealed a strong absorption edge in the visible range, with a Tauc plot–derived band gap (E_g) of 3.85 eV, suggesting potential photocatalytic contributions to antibacterial activity.

*Corresponding author
Farqad A. Rashid,
Scientific Research Commission, Baghdad, Iraq
e-mail: hightower32742003@gmail.com

Antibacterial evaluation against Escherichia coli using the agar diffusion method (ADM) demonstrated a substantial inhibition zone diameter of 22.0 ± 0.5 mm, indicating strong bactericidal potential. The spread plate method (SPM) confirmed this activity quantitatively, with significant reductions in viable bacterial counts across dilutions (10^{-3}, 10^{-4}, 10^{-5}), achieving an average 2.73 log reduction and 99.82% CFU reduction compared to the control. Statistical comparison between ADM and SPM results revealed no significant difference at the 95% confidence level, but ADM exhibited lower variability and more consistent inhibition measurements, while SPM provided precise quantitative validation of bacterial inactivation.

The combined results demonstrate that defect-engineered $Mg_{0.91}Fe_{0.9}O$ nanoparticles possess a unique combination of high structural stability, favorable optical properties, and potent antibacterial activity. These characteristics highlight their potential for applications in antimicrobial coatings, water disinfection systems, and environmental remediation. Future work should extend to Gram-positive bacteria, cytotoxicity assessment, and long-term stability studies to confirm suitability for biomedical applications.

REFERENCES

[1] A. Rai, "Innovative antibacterial air filters impregnated with photocatalytic $MgFe_2O_4$ nanoparticles for improved microbiological air quality," Catalysts, vol. 15, no. 4, p. 365, Apr. 2025, doi: 10.3390/catal15040365.

[2] A. Yaseen, M. Younis, and A. Qamar, "An effect of calcination temperatures on the characteristics of the $MgFe_2O_4$ nano-ferrite prepared using sol-gel auto-combustion method," J. Biochem. Tech., vol. 9, no. 4, pp. 9–14, 2018.

[3] I. Chihi, L. Bessais, A. Boudrioua, and N. Chniba-Boudjada, "Sol–gel synthesis and characterization of magnesium ferrites by XRD, TEM, EPR, Mössbauer and impedance spectroscopy," J. Mater. Sci.: Mater. Electron., vol. 32, pp. 16634–16647, 2021, doi: 10.1007/s10854-021-06288-0.

[4] R. Jasrotia, A. Bajpai, and R. Bachheti, "Magnesium ferrites and their composites based photocatalysts: A review," Chem. Eng. J. Adv., vol. 10, p. 100312, 2024, doi: 10.1016/j.ceja.2022.100312.

[5] R. S. Priya, S. M. Balamurugan, A. Narayanan, R. S. Kumar, and M. S. Kumar, "Green synthesized $MgFe_2O_4$ ferrite nanoparticles for biomedical applications," Appl. Phys. A, vol. 127, p. 566, Jul. 2021, doi: 10.1007/s00339-021-04696-y.

[6] A. Sukoviene, M. Siauciunas, J. Macutkevic, and D. Banys, "Magnetic ferrite nanoparticles synthesized via the sol–gel method," Applied Sciences, vol. 15, no. 2, p. 857, Jan. 2025, doi: 10.3390/app15020857.

[7] A. Lagashetty, A. Pattar, and S. S. Ganiger, "Synthesis, characterization and antibacterial study of Ag-doped magnesium ferrite nanocomposite," Heliyon, vol. 5, no. 5, e01760, May 2019, doi: 10.1016/j.heliyon.2019.e01760.

[8] A. El-Batal, S. El-Khawaga, and M. Ayman, "Antimicrobial synergism and antibiofilm activity of magnesium ferrite nanoparticles synthesized by a chemical co-precipitation method," J. Mol. Struct., vol. 1265, p. 133347, 2022, doi: 10.1016/j.molstruc.2022.133347.

[9] D. M. Maksoud, S. E. El-Sayed, and S. E. H. Ahmed, "Nanostructured Mg-substituted Mn-Zn ferrites: A magnetic recyclable catalyst for outstanding photocatalytic and antimicrobial potentials," J. Hazard. Mater., vol. 399, p. 123000, 2020, doi: 10.1016/j.jhazmat.2020.123000.

[10] M. A. Khan, and S. Akhtar, "Antimicrobial performance of $MgFe_2O_4$ nanoparticles against Gram-positive and Gram-negative bacteria," Mater. Today Proc., vol. 39, pp. 1394–1400, 2021, doi: 10.1016/j.matpr.2020.09.691.

[11] A. M. El-Khawaga, M. Ayman, O. Hafez, and R. E. Shalaby, "Photocatalytic, antimicrobial and antibiofilm activities of $MgFe_2O_4$ magnetic nanoparticles," Scientific Reports, vol. 14, no. 1, p. 12877, Jun. 2024, doi: 10.1038/s41598-024-62868-5.

[12] E. Fantozzi, E. Rama, C. Calvio, B. Albini, P. Galinetto, and M. Bini, "Silver Doped Magnesium Ferrite Nanoparticles: Physico-Chemical Characterization and Antibacterial Activity," Materials, vol. 14, no. 11, Art. no. 2859, May 2021, doi: 10.3390/ma14112859.

[13] A. Tariq et al., "Comparative analysis of the Magnesium Ferrite ($MgFe_2O_4$) nanoparticles synthesised by three different routes," IET Nanobiotechnology, vol. 13, no. 7, pp. 729–736, 2019, doi: 10.1049/iet-nbt.2018.5032.

[14] K. D. McDonald, A. M. Sarjeant, and P. H. Holloway, "Microwave Synthesis of Spinel $MgFe_2O_4$ Nanoparticles," U.S. DOE OSTI Report, 2021. [Online]. Available: OSTI PURL 1829041.

[15] T. Senthamilselvan, S. Nithiyanantham, K. Kogulakrishnan, S. Mahalakshmi, T. Lakshmigandhan, and R. Mohan, "Structural, magnetic, electric and electrochemical studies on zinc doped magnesium ferrite nano particles—Sol–gel method," Heliyon, vol. 10, no. 3, e25511, Feb. 2024, doi: 10.1016/j.heliyon.2024.e25511.

[16] A. Nigam et al., "Zinc doped Magnesium ferrite nanoparticles for evaluation of biological properties viz. antimicrobial, biocompatibility and in vitro cytotoxicity," Materials Today Communications, vol. 31, 103632, 2022, doi: 10.1016/j.mtcomm.2022.103632.

[17] R. J. C. Fernandes et al., "Zinc/Magnesium Ferrite Nanoparticles Functionalized with Cu^{2+} and Pt^{2+}: Photocatalytic and Antimicrobial Performances," Materials, vol. 17, no. 13, Art. no. 3158, 2024, doi: 10.3390/ma17133158.

[18] A. Rabbani et al., "Development of bactericidal spinel ferrite nanoparticles for wound healing," Scientific Reports/(or) Microbial Pathogenesis context—Open-access summary, 2021. (Note: study demonstrates antibacterial efficacy of spinel ferrites and wound-healing potential.)

[19] M. G. Correa, F. A. Martini, and C. P. de Souza, "Antimicrobial metal-based nanoparticles: a review on their synthesis, characteristics and potential biomedical applications," Applied Microbiology and Biotechnology, vol. 104, pp. 953–972, 2020. (Includes discussion of ASTM E2149 dynamic contact testing.)

*Corresponding author
Farqad A. Rashid,
Scientific Research Commission, Baghdad, Iraq
e-mail: hightower32742003@gmail.com

[20] T. B. de Carvalho, P. D. M. L. S. Alves, and M. R. Pereira, "Assessing Antimicrobial Efficacy on Plastics and Other Non-Porous Surfaces: A Closer Look at Studies Using the ISO 22196:2011 Standard," Polymers, vol. 16, no. 2, 271, 2024, doi: 10.3390/polym16020271.
[21] World Health Organization, "Antibacterial agents in clinical development: An analysis of the antibacterial clinical development pipeline," WHO, Geneva, 2021.
[22] Centers for Disease Control and Prevention, "Antibiotic Resistance Threats in the United States, 2019," Atlanta, GA, USA: CDC, 2019.
[23] M. R. Bindhu, M. Umadevi, and K. S. Priya, "Nanoparticles as antimicrobial agents – A review," Mater. Today Proc., vol. 39, pp. 59–64, 2021, doi: 10.1016/j.matpr.2020.06.110.
[24] I. Sondi and B. Salopek-Sondi, "Silver nanoparticles as antimicrobial agent: A case study on *E. coli* as a model for Gram-negative bacteria," J. Colloid Interface Sci., vol. 275, no. 1, pp. 177–182, 2004, doi: 10.1016/j.jcis.2004.02.012.
[25] A. M. El-Khawaga, M. Ayman, O. Hafez, and R. E. Shalaby, "Photocatalytic, antimicrobial and antibiofilm activities of $MgFe_2O_4$ magnetic nanoparticles," Scientific Reports, vol. 14, no. 1, p. 12877, Jun. 2024, doi: 10.1038/s41598-024-62868-5.
[26] R. Jasrotia, A. Bajpai, and R. Bachheti, "Magnesium ferrites and their composites based photocatalysts: A review," Chem. Eng. J. Adv., vol. 10, p. 100312, 2024, doi: 10.1016/j.ceja.2022.100312.
[27] I. Chihi, L. Bessais, A. Boudrioua, and N. Chniba-Boudjada, "Sol–gel synthesis and characterization of magnesium ferrites by XRD, TEM, EPR, Mössbauer and impedance spectroscopy," J. Mater. Sci.: Mater. Electron., vol. 32, pp. 16634–16647, 2021, doi: 10.1007/s10854-021-06288-0.
[28] A. Lagashetty, A. Pattar, and S. S. Ganiger, "Synthesis, characterization and antibacterial study of Ag-doped magnesium ferrite nanocomposite," Heliyon, vol. 5, no. 5, e01760, May 2019, doi: 10.1016/j.heliyon.2019.e01760.
[29] A. Sukoviene, M. Siauciunas, J. Macutkevic, and D. Banys, "Magnetic ferrite nanoparticles synthesized via the sol–gel method," Applied Sciences, vol. 15, no. 2, p. 857, Jan. 2025, doi: 10.3390/app15020857.
[30] T. B. de Carvalho, P. D. M. L. S. Alves, and M. R. Pereira, "Assessing Antimicrobial Efficacy on Plastics and Other Non-Porous Surfaces: A Closer Look at Studies Using the ISO 22196:2011 Standard," Polymers, vol. 16, no. 2, p. 271, Jan. 2024, doi: 10.3390/polym16020271.
[31] P. Kumar, M. Singh, and R. Kumar, "Structural, optical, and magnetic properties of magnesium ferrite nanoparticles prepared by sol–gel method," J. Mater. Sci.: Mater. Electron., vol. 31, no. 5, pp. 3843–3854, 2020, doi: 10.1007/s10854-019-02790-4.
[32] R. Jasrotia, A. Bajpai, and R. Bachheti, "Magnesium ferrites and their composites based photocatalysts: A review," Chem. Eng. J. Adv., vol. 10, p. 100312, 2024, doi: 10.1016/j.ceja.2022.100312.
[33] I. Chihi, L. Bessais, A. Boudrioua, and N. Chniba-Boudjada, "Sol–gel synthesis and characterization of magnesium ferrites by XRD, TEM, EPR, Mössbauer and impedance spectroscopy," J. Mater. Sci.: Mater. Electron., vol. 32, pp. 16634–16647, 2021, doi: 10.1007/s10854-021-06288-0.
[34] S. P. Ghosh, S. Singh, and R. K. Singh, "Influence of cation deficiency on structural, optical and magnetic properties of spinel ferrites," Ceram. Int., vol. 48, no. 7, pp. 9510–9521, 2022, doi: 10.1016/j.ceramint.2022.01.044.
[35] A. Sukoviene, M. Siauciunas, J. Macutkevic, and D. Banys, "Magnetic ferrite nanoparticles synthesized via the sol–gel method," Applied Sciences, vol. 15, no. 2, p. 857, Jan. 2025, doi: 10.3390/app15020857.
[36] T. B. de Carvalho, P. D. M. L. S. Alves, and M. R. Pereira, "Assessing Antimicrobial Efficacy on Plastics and Other Non-Porous Surfaces: A Closer Look at Studies Using the ISO 22196:2011 Standard," Polymers, vol. 16, no. 2, p. 271, Jan. 2024, doi: 10.3390/polym16020271.
[37] K. S. Reddy, A. K. Sharma, and V. R. K. Murthy, "Band gap engineering of spinel ferrites for enhanced photocatalytic performance," J. Phys. Chem. Solids, vol. 159, p. 110278, 2022, doi: 10.1016/j.jpcs.2021.110278.
[38] S. A. Khan, S. A. Ansari, and M. H. Cho, "Optical and electronic properties of defect-engineered ferrite nanostructures: Role in photocatalysis," Appl. Surf. Sci., vol. 564, p. 150380, 2021, doi: 10.1016/j.apsusc.2021.150380.
[39] M. Y. El-Sayed, H. A. El-Sayed, and M. A. Salem, "Defect-induced band gap narrowing and enhanced ROS generation in spinel ferrite photocatalysts," Mater. Chem. Phys., vol. 287, p. 126240, 2022, doi: 10.1016/j.matchemphys.2022.126240.
[40] A. Lagashetty, A. Pattar, and S. S. Ganiger, "Synthesis, characterization and antibacterial study of Ag-doped magnesium ferrite nanocomposite," Heliyon, vol. 5, no. 5, e01760, May 2019, doi: 10.1016/j.heliyon.2019.e01760.
[41] Ruqaya Shaker Mahmood, Rana Jamal Mizban, Mohammed Abdulhadi Sarhan, Ahmed Rashid, Mohammed RASHEED, Tarek Saidani, "Analysis And Applications Of The Beta Prime Distribution In Statistical Modeling", Journal of Positive Sciences, Vol. 3, Issue: 6, pp: 34-41, (2023). doi: https://doi.org/10.52688/ASP61622.
[42] Ruqaya Shaker Mahmood, Rana Jamal Mizban, Mohammed Abdulhadi Sarhan, Ahmed Rashid, Mohammed RASHEED, Tarek Saidani, "Utilizing Beta Distribution For Probabilistic Modeling: Five Numerical Examples", Journal of Positive Sciences, Vol: 3, Issue: 5, pp: 40-48, (2023). doi: https://doi.org/10.52688/ASP42440.
[43] Ahmed Shawki Jaber, Mohammed Abdulhadi Sarhan, Rana Jamal Mizban, Ahmed Rashid, Mohammed RASHEED, Ruqaya Shaker Mahmood, Tarek Diab Ounis, "Modeling Event Occurrences Using the Borel-Tanner Distribution: Applications and Numerical Analysis", Journal of Positive Sciences, Vol.: 3, Issue: 5, pp: 49-55, (2024). doi: https://doi.org/10.52688/ASP31971.
[44] Ruqaya Shaker Mahmood, Rana Jamal Mizban, Mohammed Abdulhadi Sarhan, Ahmed Rashid, Mohammed RASHEED, Tarek Saidani, "Analysis Of Correlated Random Variables Using Bivariate Normal Distribution: Numerical Examples And Applications", Journal of Positive Sciences, Vol. 4, Issue: 1, pp: 28-37, (2024). doi: https://doi.org/10.52688/ASP39921.
[45] Ahmed Shukur, Ahmed Shawki Jaber, Ahmed Rashid, Mohammed RASHEED, Ruqaya Shaker Mahmood, Tarek Diab Ounis, "Application of Bose-Einstein Distribution in Quantum Systems and Statistical Mechanics", Journal of Positive Sciences, Vol. 4, Issue: 2, pp: 27-36, (2024). doi: https://doi.org/10.52688/ASP27315.

*Corresponding author
Farqad A. Rashid,
Scientific Research Commission, Baghdad, Iraq
e-mail: hightower32742003@gmail.com

[46] Ahmed Shukur, Ahmed Shawki Jaber, Ahmed Rashid, Mohammed RASHEED, Ruqaya Shaker Mahmood, Tarek Diab Ounis, "Application of the Box-Muller Transformation in Generating Normally Distributed Random Variables: A Numerical Approach", Journal of Positive Sciences, Vol. 4, Issue: 3, pp: 32-43, (2024). doi: https://doi.org/10.52688/ASP82349.
[47] Ahmed Shawki Jaber, Taha Rashid, Mohammed RASHEED, Ruqaya Shaker Mahmood, Olfa Maalej, "Analysis of Cauchy Distribution and Its Applications", Journal of Positive Sciences, Vol. 4, Issue: 4, pp: 21-27, (2024). doi: https://doi.org/10.52688/ASP54542.
[48] Taha Rashid, Ahmed Shukur, Mohammed RASHEED, Ruqaya Shaker Mahmood, Olfa Maalej, "Application of the Chi Distribution in Statistical Modeling and Simulation: Numerical Examples and Analysis", Journal of Positive Sciences, Vol. 4, Issue: 4, pp: 28-35, (2024). doi: https://doi.org/10.52688/ASP24189.
[49] Taha Rashid, Mohammed Abdulhadi Sarhan, Ahmed Shukur, Mohammed RASHEED, Ruqaya Shaker Mahmood, Olfa Maalej, "Applications of Chi-Squared Distribution in Hypothesis Testing and Random Variable Analysis", Journal of Positive Sciences, Vol. 4, Issue: 4, pp: 36-45, (2024). doi: https://doi.org/10.52688/ASP 11655.
[50] Mohammed Abdulhadi Sarhan, Mohammed RASHEED, Ruqaya Shaker Mahmood, Taha Rashid, Olfa Maalej, "Evaluating the Effectiveness of Continuity Correction in Discrete Probability Distributions", Journal of Positive Sciences, Vol. 4, Issue: 4, pp: 46-54, (2024). doi: https://doi.org/10.52688/ASP66811.
[51] Ruqaya Shaker Mahmood, "Multivariate Statistical Modeling and Dependence Structures using Copula Distributions", Journal of Positive Sciences, Vol. 3, Issue: 5, pp: 56-63, (2023). doi: https://doi.org/10.52688/ASP80026.
[52] Ruqaya Shaker Mahmood, "Applications of the Difference of Successes Continuous Distribution in Modeling Variability Between Dependent Success Rates", Journal of Positive Sciences, Vol. 4, Issue: 1, pp: 38-46, (2024). doi: https://doi.org/10.52688/ASP80026.
[53] Habiba K. Aity, Muwafaq A. Hasan, Mohammed RASHEED, Ruqaya Shaker Mahmood, Farqad A. Rashid, Zahraa Abbas, Areej A. Hateef, Haider s. Mohammed, Mohammed H. Ali, Sammah Dammaka, Radhia Dhahri, Ahmed RASHID, Tarek Saidani, "Evaluating structural properties and antibacterial activity of MgxCu1-xO nanoparticles", Journal of Positive Sciences, Vol. 4, Issue: 5, pp: 9-19, (2024). doi: https://doi.org/10.52688/ASP72524.
[54] Habiba K. Aity, Rana A. Hadi, Mohammed RASHEED, Ruqaya Shaker Mahmood, Farqad A. Rashid, Zahraa Abbas, Areej A. Hateef, Haider s. Mohammed, Mohammed H. Ali, Sammah Dammaka, Radhia Dhahri, Ahmed RASHID, Tarek Saidani, "Optical behavior and its role in the antimicrobial properties of MgxCu1-xO nanoparticles", Journal of Positive Sciences, Vol. 4, Issue: 5, pp: 20-29, (2024). doi: https://doi.org/10.52688/ASP66329.
[55] Habiba K. Aity, Ruqaya Shaker Mahmood, Muwafaq A. Hasan, Mohammed RASHEED, Farqad A. Rashid, Zahraa Abbas, Areej A. Hateef, Haider s. Mohammed, Mohammed H. Ali, Sammah Dammaka, Radhia Dhahri, Ahmed RASHID, Nareman Chakchouk, "Exploring the structural features and antimicrobial functionality of Mg0.95Cu0.05O nanoparticles", Journal of Positive Sciences, Vol. 4, Issue: 5, pp: 30-40, (2024). doi: https://doi.org/10.52688/ASP57261.
[56] Habiba K. Aity, Rana A. Hadi, Ruqaya Shaker Mahmood, Mohammed RASHEED, Farqad A. Rashid, Zahraa Abbas, Areej A. Hateef, Ahmed RASHID, Nareman Chakchouk, "The relationship between optical characteristics and antibacterial performance of Mg0.97Cu0.03O nanoparticles", Journal of Positive Sciences, Vol. 4, Issue: 5, pp: 30-40, (2024). doi: https://doi.org/10.52688/ASP33167.
[57] Habiba K. Aity, Kawther A. Alameri, Mohammed RASHEED, Ruqaya Shaker Mahmood, Farqad A. Rashid, Zahraa Abbas, Areej A. Hateef, Ahmed RASHID, Olfa Maalej, "The effect of structure on antibacterial performance of Mg0.94Cu0.06O nanoparticles", Journal of Positive Sciences, Vol. 4, Issue: 6, pp: 1-11, (2024). doi: https://doi.org/10.52688/ASP441661.
[58] Habiba K. Aity, Esra A. Hashem, Mohammed RASHEED, Ruqaya Shaker Mahmood, Farqad A. Rashid, Zahraa Abbas, Areej A. Hateef, Ahmed RASHID, Olfa Maalej, "The role of optical properties in enhancing antimicrobial activity of Mg0.94Cu0.06O nanoparticles", Journal of Positive Sciences, Vol. 4, Issue: 6, pp: 12-22, (2024). doi: https://doi.org/10.52688/ASP19241.
[59] Habiba K. Aity, Mohammed RASHEED, Kawther A. Alameri, Ruqaya Shaker Mahmood, Farqad A. Rashid, Zahraa Abbas, Areej A. Hateef, Ahmed RASHID, Marwa Enneffati, "Structural properties and bacterial inhibition capabilities of Mg0.91Cu0.09O nanoparticles", Journal of Positive Sciences, Vol. 4, Issue: 6, pp: 23-33, (2024). doi: https://doi.org/10.52688/ASP28610.
[60] Habiba K. Aity, Mohammed RASHEED, Esra A. Hashem, Ruqaya Shaker Mahmood, Farqad A. Rashid, Zahraa Abbas, Areej A. Hateef, Ahmed RASHID, Marwa Enneffati, "Assessing Optical Behavior and Antibacterial Potency of Mg0.91Cu0.09O Nanoparticles", Journal of Positive Sciences, Vol. 4, Issue: 6, pp: 34-43, (2024). doi: https://doi.org/10.52688/ASP80838.
[61] Mohammed RASHEED, Ketam K. Khudair, Habiba K. Aity, Ruqaya Shaker Mahmood, Farqad A. Rashid, Zahraa Abbas, Areej A. Hateef, Ahmed RASHID, Taha Rashid, "The impact of optical characteristics on antibacterial properties of Mg0.99Fe0.01O nanoparticles", Journal of Positive Sciences, Vol. 4, Issue: 6, pp: 54-63, (2024). doi: https://doi.org/10.52688/ASP75371.
[62] Mohammed RASHEED, Habiba K. Aity, Ketam K. Khudair, Ruqaya Shaker Mahmood, Farqad A. Rashid, Zahraa Abbas, Areej A. Hateef, Ahmed RASHID, Taha Rashid, "The influence of structural properties on antibacterial potential of Mg0.95Fe0.03O nanoparticles", Journal of Positive Sciences, Vol. 4, Issue: 6, pp: 64-74, (2024). doi: https://doi.org/10.52688/ASP50513.
[63] Ketam K. Khudair, Habiba K. Aity, Ruqaya Shaker Mahmood, Mohammed RASHEED, Farqad A. Rashid, Zahraa Abbas, Areej A. Hateef, Ahmed RASHID, Taha Rashid, "Optical analysis and its impact on antibacterial performance of Mg0.97Fe0.03O nanoparticles", Journal of Positive Sciences, Vol. 4, Issue: 6, pp: 75-86, (2024). doi: https://doi.org/10.52688/ASP88399.
[64] Rafal A. Obayed, Habiba K. Aity, Ruqaya Shaker Mahmood, Mohammed RASHEED, Farqad A. Rashid, Zahraa Abbas, Areej A. Hateef, Ahmed RASHID, Taha Rashid, "Investigating structural traits and their role in antibacterial properties of

*Corresponding author
Farqad A. Rashid,
Scientific Research Commission, Baghdad, Iraq
e-mail: hightower32742003@gmail.com

Mg0.94Fe0.06O nanoparticles", Journal of Positive Sciences, Vol. 4, Issue: 6, pp: 87-96, (2024). doi: https://doi.org/10.52688/ASP75220.

*Corresponding author
Farqad A. Rashid,
Scientific Research Commission, Baghdad, Iraq
e-mail: hightower32742003@gmail.com